Journal of Fluids and Structures (2002) **16**(4), 487–495
doi:10.1006/jfls.2001.0432, available online at http://www.idealibrary.com on IDEAL®

NUMERICAL RESEARCH ON THE COHERENT STRUCTURES IN A MIXING LAYER WITH CROSS-SHEAR

J.-Z. LIN, Z.-S. YU, X.-M. SHAO

State Key Laboratory of Fluid Power Transmission and Control
Department of Mechanics, Zhejiang University, Hangzhou, 310027
People's Republic of China

(Received 8 July 1999; and in final form 2 October 2001)

The evolution of a time-developing mixing layer with cross-shear is simulated numerically using a pseudo-spectral method. The results indicate that stretching by the rollers is responsible for the formation of the streamwise vortices in a mixing layer with cross-shear. When the cross-shear is relatively strong (such as $\theta = 20^\circ$), the co-rotating streamwise vortices related to the early spanwise Kelvin–Helmholtz instability are intensified rapidly by stretching and collapse into rib-shaped vortices, which are very similar to the ribs in a plane mixing layer. At $\theta = 20^\circ$, the vortex corresponding to the "quadrupole" in a plane mixing layer is also observed in the core region, and a set of streamwise vortices with signs opposite to those of the vortices containing the ribs lie at the spanwise braid region. The counterparts of the ribs, however, are of flat shape and much weaker. When θ is up to 30°, the ribs are so strong that their counterparts cannot develop. When θ is down to 10°, the symmetry of the streamwise vortices is more obvious, but the ribs do not form. Additionally, it is revealed that the introduction of the strong cross-shear results in enhanced mixing compared to a two-dimensional mixing layer.

1. INTRODUCTION

THE MIXING LAYER IS AN IMPORTANT MODEL for the study of turbulence in free shear layers and is commonly encountered in various natural flows and industrial equipment such as a combustor. Hence, investigations on the coherent structures in mixing layers are of great significance from both theoretical and practical points of view and have aroused considerable attention among turbulence researchers over the past three decades. Extensive experimental [see, e.g., Lasheras & Choi (1988)] and numerical [see, e.g., Rogers & Moser (1992)] studies show that there are coherent structures in a plane mixing layer, known as the spanwise vortices (rollers) as a result of Kelvin-Helmholtz instability and the secondary counter-rotating streamwise vortices (ribs) caused by the stretching of the spanwise vortices. The quadrupoles with sign opposite to that of the ribs are also important streamwise vortices. They develop at the core region and are mainly responsible for the evolution of the rollers into cup-shaped vortices, as shown in the work of Rogers & Moser (1992) (referred to as RM henceforth). More recently, Leboeuf & Mehta (1996) have observed the quadrupoles in their experiments.

The vortical structures mentioned above are discovered in a plane mixing layer, in which the top and bottom streams are parallel to each other. If the two streams are not parallel, the flow will undergo cross-shear. It is necessary to understand the features and the

0889–9746/02/040487 + 09 $35.00/0

formation mechanics of the coherent structures in this special flow because it is common in flows of ocean and air currents. So far, however, few studies have been performed on it. Lin & Wei (1993) and Lin & Wang (1997) conducted the experiments and the numerical simulations, but they did not present the characteristics of the coherent structures. The main achievements have been attained by Atsavapranef & Gharib (1994) (referred to as henceforth AG). They did the experiments in a flat tank and made stratified mixing layer flows with cross-shear by tilting the tank. AG observed a new type of structure, namely co-rotating streamwise vortices, which first appeared in the braids and then extended toward the cores. Although their results indicate that the wave number of the spanwise instability nearly equals that of the primary Kelvin–Helmholtz instability and the streamwise vortices can pair, like the spanwise rollers, AG suggested that the flows are not two separate and independent sets of perpendicular Kelvin–Helmholtz instability superimposed upon each other; rather, the streamwise vortices are manifestations of an instability of the Kelvin–Helmholtz braid. However, AG neither discussed the mechanics of the braid instability nor presented the detailed streamwise vortical structures (it is a difficult task in experimental studies). Here, we simulate the formation and evolution of the coherent structures in a mixing layer with cross-shear of various intensities numerically and analyse the mechanics for the formation of secondary structures.

2. NUMERICAL MODEL

Figure 1 shows a schematic of a mixing layer with cross-shear. Here, let 2θ designate the intersection angle of the two streams. For convenience in describing, we refer to the main shear direction (X) as streamwise and another shear direction (Z) as spanwise, the terms borrowed from a plane mixing layer. A time-developing mixing layer can be taken as the numerical model in this study, because it may be thought of as an approximation to the evolution of a single set of flow structures as they are convected downstream in the spatially developing mixing layer as suggested by RM, and a similar evolution of vortical structures also exists in a cross-shear mixing layer. Periodic boundary conditions can be imposed in the streamwise and spanwise directions for a time-developing mixing layer. The spatially developing mixing layers are more common, however, the experimental model of AG is closer to the time-developing flow. Therefore, a comparison between the results of this paper and AG is reasonable.

The main stream velocity difference U is taken as the characteristic velocity, and twice the initial momentum thickness δ_0 as the characteristic length; thus, the Reynolds number is defined by $\mathrm{Re} = U\delta_0/\nu$.

The initial streamwise and spanwise velocity fields are given respectively, as follows:

$$u = \cos(\theta)[0{\cdot}5\tanh(y) + A\Re(\phi'(y)\mathrm{e}^{\mathrm{i}\alpha x})], \tag{1}$$

$$w = \sin(\theta)[0{\cdot}5\tanh(y) + A\Re(\phi'(y)\mathrm{e}^{\mathrm{i}\beta z})], \tag{2}$$

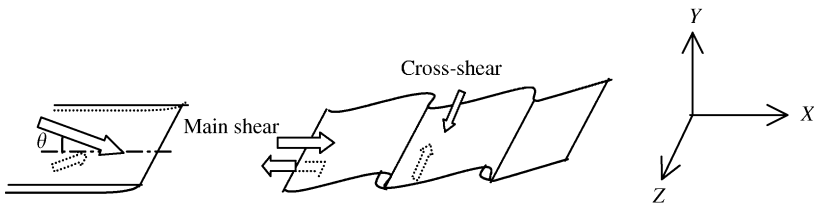

Figure 1. Schematic of a mixing layer with cross-shear.

where A is the disturbance amplitude, α the streamwise wave number, and β the spanwise wave number; ϕ denotes the normalized eigenfunction, which can be derived from linear stability theory. The symbol $\Re$ signifies the real part for a complex function, and the prime designates differentiation. In this study, the value of α is set to be 0·4446 and that of β is set to be 0·5. We fix $A = 0{\cdot}1$ throughout this paper.

In the experiments of AG, the very low and broad-band disturbances are introduced naturally, whereas in this paper, just low wave number disturbances with a certain form are imposed initially. However, it does not make a large difference for the evolution of mixing layer. The choice of the streamwise and spanwise wavelengths in this paper is suitable because the momentum thickness grows fastest for the case when the two wavelengths are of the same order, and the most amplified disturbance predominates in the evolution of a mixing layer. Additionally, a small disturbance method is used in the study of spanwise and streamwise instabilities in this paper. Therefore, Fourier mode energies are not examined, but may be helpful in the study of instability.

To simplify the computation, we impose the periodic condition in the transverse direction by introducing the image flows far enough from the mixing layer centre. The streamwise period $L_1$is taken to be $2\pi/\alpha$, the transverse period L_2 is 32, and spanwise period L_3 is $2\pi/\beta$.

The governing equations are

$$\nabla \cdot \boldsymbol{V} = 0, \tag{3}$$

$$\frac{\partial \boldsymbol{V}}{\partial t} + \nabla\left(p + \frac{|\boldsymbol{V}|^2}{2}\right) = \boldsymbol{V} \times \omega + \frac{\nabla^2 \boldsymbol{V}}{\mathrm{Re}}. \tag{4}$$

The passive scalar is determined from

$$\frac{\partial T}{\partial t} + \boldsymbol{V} \cdot \nabla T = \frac{\nabla^2 T}{\mathrm{Pe}}, \tag{5}$$

where Pe denotes Peclet number, defined by $\mathrm{Pe} = \mathrm{Re}\,\mathrm{Sc}$, here $\mathrm{Sc} = \nu/\gamma$ (γ being the molecular diffusivity of the scalar). The value of Re and Sc are taken to be 200 and 2, respectively, in the paper.

The initial passive scalar is given by

$$T = 0{\cdot}5(1 + \tanh y). \tag{6}$$

Equations (3)–(5) are solved with the standard pseudo-spectral method; equations (4) and (5) are advanced in time with the Adams–Bashforth–Crank–Nicolson scheme. The time step, the period in the transverse direction and the number of Fourier modes are fixed to be 0·05, 32 and $64 \times 128 \times 64$, respectively. The above parameters are chosen after a number of preliminary tests and are based on the following two considerations. One is making the resolution to a large extent dictated by the available computational resources. The other is ensuring the convergence of computation. The values of time step, L_2, and the mesh size used in our study are appropriate because they not only result in modest computation but ensure enough accuracy in the solution. In fact, we can refer to the work of Azaiez & Homsy (1994) (referred to as AH below) and Kumar & Homsy (1999) (KH) on the choice of these values since their models are similar to ours, except that we considered the cross-shear case. AH typically used 0·04, 8 and 128×128 to simulate the roll-up of 2-D viscoelatic mixing layers and KH used 0·02, 12 and $128 \times 128 \times 64$ for the 3-D Newtonian case. They employed a little bit finer time step and mesh size as compared to ours; but we found $\mathrm{d}t = 0{\cdot}05$ is small enough, which is understandable since we used a second-order accurate time scheme. Our mesh resolution is also sufficient since we used the spectral method and actually most of

energy of the fluid field is contributed by very low wave number modes before the advent of turbulence. KH chose $L_2 = 12$, which is much smaller than ours (32) but may be enough for their study, as they only focused on the linear instability phase. The value $L_2 = 32$ is large enough for the study of the non-linear instability before turbulence appears, which is what we examined in our study.

3. RESULTS AND DISCUSSION

We analyse the vortical structure in reference to vorticity contours on the following four planes: $X = 0$ (middle at the streamwise braids), $X = L_1/2$ (middle at the streamwise cores),

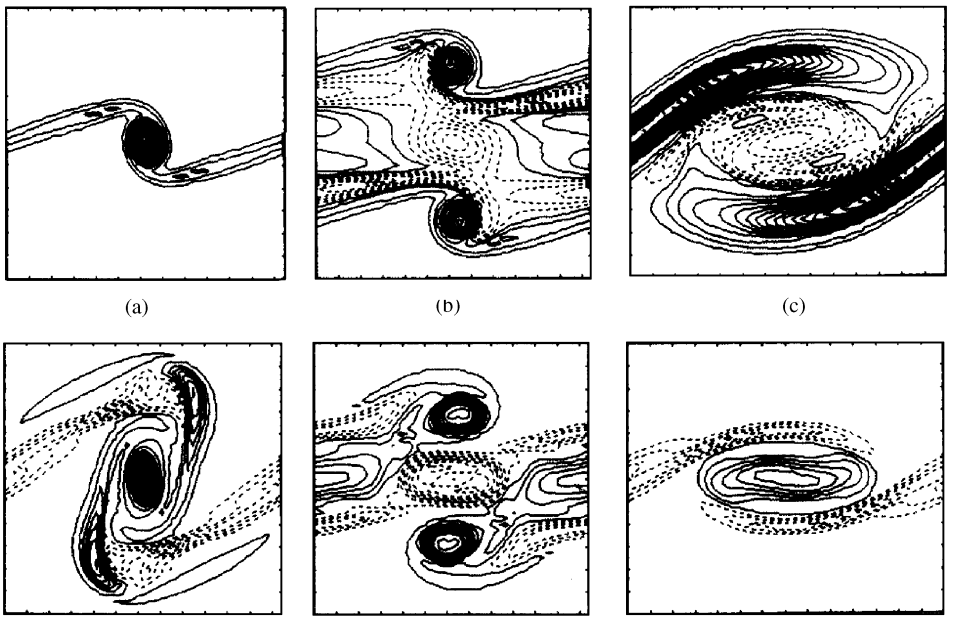

Figure 2. Contours of the streamwise vorticity at $\theta = 20^\circ$: (a) $t = 50$, on $X = 0$ plane, minimum contour = 0·05, maximum contour = 1·55; (b) $t = 50$, on $X = L_1/2$ plane, minimum contour = $-0{\cdot}38$, maximum contour = 1·09; (c) $t = 50$, on $Z = L_3/2$ plane, minimum contour = $-0{\cdot}38$, maximum contour = 1·58; (d) $t = 60$, on $X = 0$ plane, minimum contour = $-0{\cdot}37$, maximum contour = 1·36; (e) $t = 60$, on $X = L_1/2$ plane, minimum contour = $-0{\cdot}66$, maximum contour = 0·88; (f) $t = 60$, on $Z = 0$ plane, minimum contour = $-0{\cdot}30$, maximum contour = 0·42.

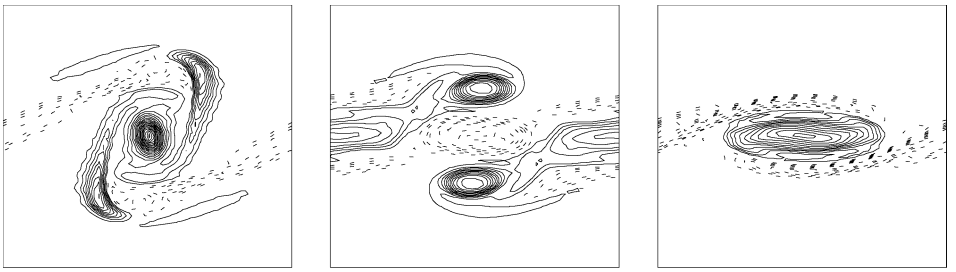

Figure 3. Contours of the streamwise vorticity at $\theta = 20^\circ$ (comparing with Figure 2): (a) $t = 60$, on $X = 0$ plane, minimum contour = $-0{\cdot}37$, maximum contour = 1·37; (b) $t = 60$, on $X = L_1/2$ plane, minimum contour = $-0{\cdot}66$, maximum contour = 0·89; (c) $t = 60$, on $Z = 0$ plane, minimum contour = $-0{\cdot}30$, maximum contour = 0·42.

$Z = 0$ (middle at the spanwise braids) and $Z = L_3/2$ (middle at the spanwise cores). Actually, the contours on these plane can reflect the main characteristics of the vortices. Figure 2 shows the contours of streamwise vorticity for $\theta = 20^\circ$ at $t = 50$ and 60. We also did a convergence test by varying the mesh size (e.g., $128 \times 128 \times 64$, a finer mesh than that limited by our computer resources); Figure 3 shows the results corresponding to Figure 2. Quantitative differences among them were found to be small, by comparing the two figures, which demonstrates that calculations have converged. The contours of spanwise vorticity are shown in Figure 4. Figures 5 and 6 are the vorticity contours for $\theta = 10$ and 30°, respectively. The value of θ determines the intensity of cross-shear. "The braids" (or the "cores"), when not specified, means "the streamwise braids" (or "the streamwise cores") in what follows.

For $\theta = 20^\circ$, the co-rotating concentrated streamwise vortices have appeared at the braids by $t = 50$ (Figure 2), extending to the cores roughly along the edge of the rollers (direction of the stretching axes). The structures are very similar to the ribs in a plane mixing layer (see RM). Moreover, the streamwise vortices in the cores are also similar to the quadrupoles. These similarities indicate that the stretching by the spanwise vortices, not the spanwise Kelvin–Helmholtz instability, is responsible for the formation of the streamwise vortices in a mixing layer with cross-shear. The experiments of AG substantiate this point. As mentioned in the introduction herein, AG found that the co-rotating streamwise vortices first appear in the braids and then extend toward the cores. Hence, AG suggested that the flows are not two separate and independent sets of perpendicular Kelvin–Helmholtz instabilities superimposed upon each other; rather, the streamwise vortices are manifestations of an instability of the Kelvin–Helmholtz braid. It is well-known that the braids are regions of the most intense stretching. For a plane mixing layer, the disturbances of a sine/cosine type in the spanwise direction will evolve into the counter-rotating streamwise pairs by stretching, and the structures are spanwise symmetric. When cross-shear is introduced, it is conceivable that Kelvin–Helmholtz instabilities occur in two directions in the early stages since the intensity is the sole difference. The spanwise vortices roll up firstly because of the predominance in the streamwise direction, which produces strong stretching and causes the rapid development of the streamwise vortices. However, the streamwise structures formed are different with different intensities of cross-shear.

When the cross-shear is weak, the initial spanwise Kelvin–Helmholtz instability is also weak, and the streamwise vortices resemble those in a plane mixing layer in that the symmetry develops to some extent. For $\theta = 10^\circ$, the co-rotating streamwise vortices related to the initial spanwise Kelvin–Helmholtz instability appear on the $X = 0$ plane at $t = 50$, but they are clearly weak (Figure 5). By $t = 80$, the counter-rotating vortices have emerged at the spanwise braids on the $X = 0$ plane, and the symmetry of the structures is more obvious at the cores. Additionally, the strong and concentrated circular vortices cannot form. Consequently, the main role of weak cross-shear is that it delays the development of symmetric structures in a plane mixing layer and especially inhibits the formation of the ribs.

When the cross-shear is strong enough (such as $\theta = 30^\circ$), the spanwise Kelvin–Helmholtz instability produces the relatively strong co-rotating streamwise vortices, which collapse quickly into the ribs by stretching (Figure 6). The co-rotating ribs are so predominant that their counterparts are completely inhibited. Furthermore, they stretch the streamwise vortices between them in the cores into a flat shape ($t = 80$ in Figure 6).

The vortical structures for $\theta = 20^\circ$ have similar features as those of the above two cases. The co-rotating ribs have formed by $t = 50$ (Figure 2) and then there is a tendency for the streamwise structures to develop towards the symmetric type. The counterparts of the ribs can be observed at $t = 60$ in Figure 4. They, however, cannot collapse, being flat in shape and much weaker.

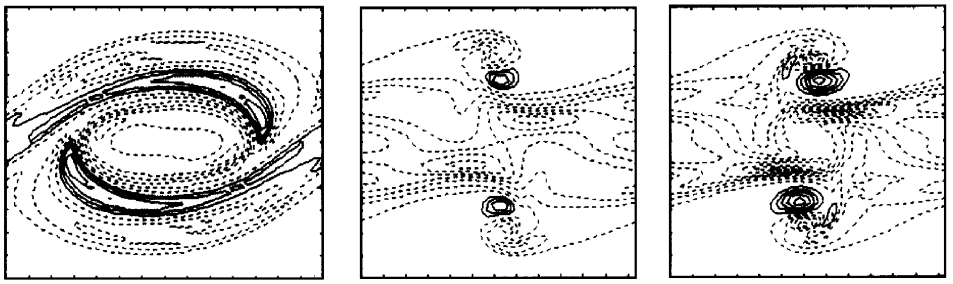

Figure 4. Contours of the spanwise vorticity at $\theta = 20°$: (a) $t = 50$, on $Z = L_3/2$ plane, minimum contour $= -0{\cdot}50$, maximum contour $= 0{\cdot}22$; (b) $t = 50$, on $X = L_1/2$ plane, minimum contour $= -0{\cdot}52$, maximum contour $= 0{\cdot}14$; (*c*) $t = 60$, on $X = L_1/2$ plane, minimum contour $= -0{\cdot}67$, maximum contour $= 0{\cdot}34$.

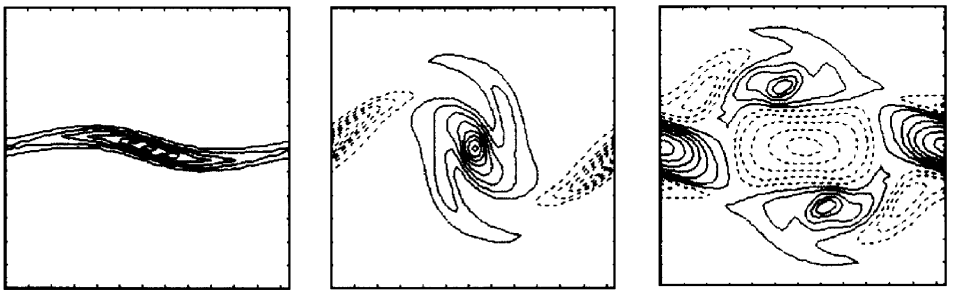

Figure 5. Contours of the streamwise vorticity at $\theta = 10°$: (a) $t = 50$, on $X = 0$ plane, minimum contour $= 0{\cdot}05$, maximum contour $= 0{\cdot}41$; (b) $t = 80$, on $X = 0$ plane, minimum contour $= -0{\cdot}55$, maximum contour $= 0{\cdot}66$; (c) $t = 80$, on $X = L_1/2$ plane, minimum contour $= -0{\cdot}38$, maximum contour $= 0{\cdot}53$.

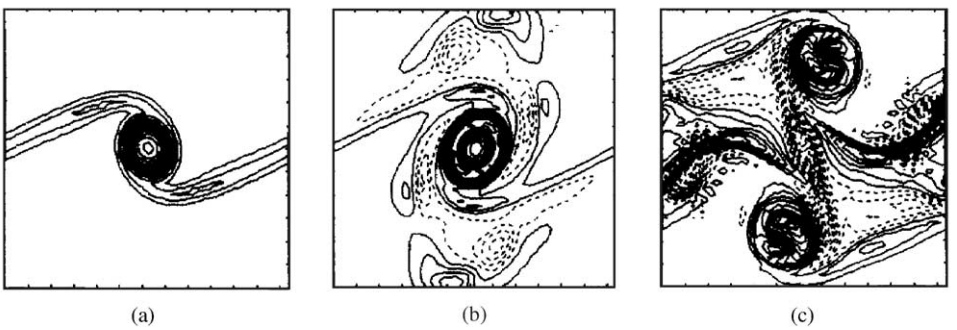

Figure 6. Contours of the streamwise vorticity at $\theta = 30°$: (a) $t = 40$, on $X = 0$ plane, minimum contour $= 0{\cdot}05$, maximum contour $= 1{\cdot}16$; (b) $t = 70$, on $X = 0$ plane, minimum contour $= -0{\cdot}30$, maximum contour $= 0{\cdot}82$; (c) $t = 80$, on $X = L_1/2$ plane, minimum contour $= -1{\cdot}20$, maximum contour $= 1{\cdot}07$.

The cross-shears of different intensities result in the streamwise structures of different types, and thereby cause the distinct spanwise structures due to strong interactions of the streamwise and spanwise vortices. The stretching and wrapping of the spanwise vortices by

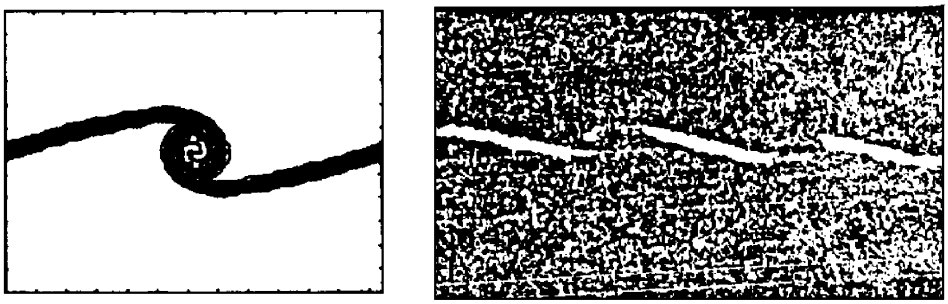

(a) (b)

Figure 7. Contours of the passive scalar on $X = 0$ plane ($\theta = 20^\circ$, $t = 50$): (a) result of numerical simulation; (b) experimental streaks (from AG) showing the co-rotating streamwise vortices.

the streamwise ones is most notable. In the case of $\theta = 20^\circ$, the ribs apparently wrap the spanwise vorticity around them and induce the spanwise vorticity with sign opposite to that of the rollers (Figure 4). Meanwhile, the spanwise vorticity at the core region between the ribs and the quadrupoles grows because of their stretching, which is just the reason for the formation of the cup-shaped vortices in a plane mixing layer.

As a result, not only the mechanics for the formation of the streamwise vortices, but also that for the interaction of the vortices, is the same for a mixing layer with and without cross-shear. However, the introduction of cross-shear destroys the symmetry of the structures and renders the structures more complex.

Figure 7 shows the contours of the passive scalar calculated here at $t = 50$ for $\theta = 20^\circ$ and the experimental streaks from AG. Both reveal the co-rotating and concentrated streamwise vortices, indicating that our results are reasonable.

AG found that the co-rotating streamwise vortices can result in an enhanced mixing, however, they form only when cross-shear is introduced after the primary shear layer has started to roll-up. The reason, they suggested, is that the streamwise vortices are an instability of the braid, and the braid needs to be setup in order for the streamwise instability to develop. Moreover, the level of cross-shear is high enough (ratio to that of main shear is larger than 0·15 for the case examined) to induce them. Our calculated results confirm that the strong co-rotating streamwise vortices (ribs) can not form for the weak cross-shear; however, they discredit the first condition above because cross-shear is introduced at the initial time for each case in this study. From a theoretical perspective, our results are more reasonable, because the forming rollers can also produce strong stretching at the forming braids. The disagreement is not surprising, since the experimental and the simulated flows are not completely consistent; for instance, the former is a type of stratified flow and not subjected to forced disturbances.

The study by AG quantifies mixing by computing the mixed-fluid thickness in terms of the density field on a plane (for its physical meaning, see AG). Here, we define it in terms of the three-dimensional passive scalar field as

$$\delta_m = \int_{-L_2/2}^{L_2/2} \frac{\int_0^{L_1}\int_0^{L_3} H(T-\bar{T})(T_t - T)\mathrm{d}x\mathrm{d}z + \int_0^{L_1}\int_0^{L_3} \mathrm{H}(\bar{T}-T)(T-T_b)\mathrm{d}x\mathrm{d}z}{\int_0^{L_1}\int_0^{L_3} H(T-\bar{T})(T_t-\bar{T})\mathrm{d}x\mathrm{d}z + \int_0^{L_1}\int_0^{L_3} H(\bar{T}-T)(\bar{T}-T_b)\mathrm{d}x\mathrm{d}z}\mathrm{d}y, \qquad (7)$$

in which T_t, T_b and $\bar{T}$ represent the levels of the passive scalar for the top and bottom fluids, and their average, respectively. In this study, $T_t = 1$, $T_b = 0$ and $\bar{T} = 0{\cdot}5$, according to

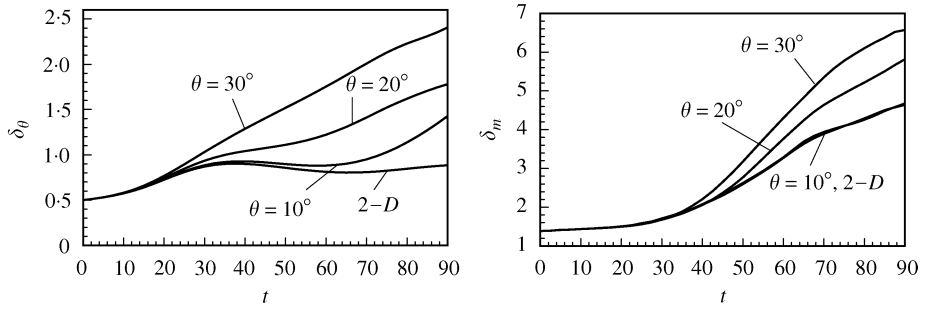

Figure 8. Time development of the mean momentum thickness δ_θ and the mixed-fluid thicknessδ_m.

equation (6). The term H is the Heaviside step function, defined as

$$H(f) = \begin{cases} 1 & f \geq 0, \\ 0 & f < 0\,. \end{cases} \tag{8}$$

The mean momentum thickness, similar to the no-cross-shear mixing layer [e.g., see Rogers & Moser (1992)], is defined as

$$\delta_\theta = \int_{-\infty}^{+\infty} (0.25 - \bar{U}^2)\mathrm{d}y, \tag{9}$$

where $\bar{U}$ denotes the total mean velocity.

Figure 8 shows the time developments of mean momentum thickness and mixed-fluid thickness in a mixing layer with cross-shear and a two-dimensional one. Compared to the two-dimensional case, the two thicknesses grow more rapidly after roll-up for the strong cross-shear case, whereas there is no gain in mixing for the weak cross-shear case. This is consistent with the results of AG.

4. CONCLUSIONS

From the foregoing discussion, stretching by the rollers is responsible for the formation of the streamwise vortices in a mixing layer with cross-shear. When the cross-shear is relatively intense (such as $\theta = 20°$), the co-rotating streamwise vortices related to the early spanwise Kelvin–Helmholtz instability are intensified rapidly by stretching and collapse into rib-shaped vortices, which are very similar to the ribs in a plane mixing layer. At $\theta = 20°$, the vortex corresponding to the "quadrupole" in a plane mixing layer is also observed in the core region, and a set of streamwise vortices with signs opposite to those of the vortices containing the ribs lie at the spanwise braid region. The counterparts of the ribs, however, are flat in shape and much weaker. When θ is up to $30°$, the ribs are so strong that their counterparts cannot develop. When θ is down to $10°$, the symmetry of the streamwise vortices is more obvious, but the ribs do not form. Consequently, introducing weak cross-shear is not judicious if enhancing mixing is of interest, since the ribs play an important role in mixing. Additionally, the computations reveal that the introduction of the strong cross-shear results in enhanced mixing compared to a two-dimensional mixing layer.

ACKNOWLEDGEMENTS

This work was supported by the National Natural Science Foundation for Outstanding Youth of China.

References

ATSAVAPRANEE, P. & GHARIB, M. 1994 A plane mixing layer with cross shear. *Physics of Fluids*, 2880–2882.

AZAIEZ, J. & HOMSY, G. M. 1994 Numerical simulation of non-Newtonian free shear flows at high Reynolds numbers. *Journal of Non-Newtonian Fluid Mechanics* **52,** 333–374.

KUMAR, S. & HOMSY, G. M 1999 Direct numerical simulation of hydrodynamic instabilities in two- and three-dimensional viscoelastic free shear layers. *Journal of Non-Newtonian Fluid Mechanics* **83,** 249–276.

LASHERAS, J. C. & CHOI, H. 1988 Three-dimensional instability of a plane free shear layer: an experimental study of the formation and evolution of streamwise vortices. *Journal of Fluid Mechanics* **189,** 53–86.

LEBOEUF, R. L. & MEHTA, R. D. 1996 Vortical structure morphology in the region of a forced mixing layer: roll-up and pairing. *Journal of Fluid Mechanics* **315,** 175–221.

LIN, J. Z. & WANG, C. X. 1997 Numerical simulation of free mixing layer with the second cross shear. *Journal of Northwest Institute of Textile Science and Technology*, **11** (Suppl), 1–4 (in Chinese).

LIN, J. Z. & WEI, Z. L. 1993 Experimental research on a free-shear layer with cross-shear. *Experimental Mechanics* **8,** 3–69 (in Chinese).

ROGERS, M. M. & Moser, R. D. 1992 The three-dimensional evolution of a plane mixing layer: the Kelvin–Helmholtz rollup. *Journal of Fluid Mechanics* **243,** 183–226.